Upscaling the diffusion equations in particulate media made of highly conductive particles. II. Application to fibrous materials

J.-P. Vassal, L. Orgéas,* D. Favier, and J.-L. Auriault
Laboratoire Sols-Solides-Structures (3S), CNRS-Universités de Grenoble (INPG-UJF), BP 53, 38041 Grenoble cedex 9, France

S. Le Corre
GeM-Institut de Recherche en Génie Civil et Mécanique, CNRS-Ecole Centrale de Nantes, BP 92101, 44321 Nantes cedex 3, France
(Received 22 August 2007; published 7 January 2008)

In paper I [Vassal *et al.*, Phys. Rev. E **77**, 011302 (2008)] of this contribution, the effective diffusion properties of particulate media with highly conductive particles and particle-particle interfacial barriers have been investigated with the homogenization method with multiple scale asymptotic expansions. Three different macroscopic models have been proposed depending on the quality of contacts between particles. However, depending on the nature and the geometry of particles contained in representative elementary volumes of the considered media, localization problems to be solved to compute the effective conductivity of the two first models can rapidly become cumbersome, time and memory consuming. In this second paper, the above problem is simplified and applied to networks made of slender, wavy and entangled fibers. For these types of media, discrete formulations of localization problems for all macroscopic models can be obtained leading to very efficient numerical calculations. Semianalytical expressions of the effective conductivity tensors are also proposed under simplifying assumptions. The case of straight monodisperse and homogeneously distributed slender fibers with a circular cross section is further explored. Compact semianalytical and analytical estimations are obtained when fiber-fiber contacts are perfect or very poor. Moreover, two discrete element codes have been developed and used to solve localization problems on representative elementary volumes for the same types of contacts. Numerical results underline the significant roles of the fiber content, the orientation of fibers as well as the relative position and orientation of contacting fibers on the effective conductivity tensors. Semianalytical and analytical predictions are discussed and compared with numerical results.

DOI: 10.1103/PhysRevE.77.011303 PACS number(s): 81.05.Rm, 81.05.Qk, 44.05.+e, 45.05.+x

I. INTRODUCTION

Improving thermal or electrical conductivity of polymer composites using highly conductive particles made of carbon (carbon black, fibers or nanotubes), aluminum (powder or fibers) or copper (powder or fibers) becomes an interesting solution for industrial applications like heat sinks, electronic components, breaking systems, etc. Within that context, fibrous conductive particles are of great interest, since the formation of a connected cluster that crosses samples and enhances conduction may appear for a very low volume fraction of fibers. However, diffusion phenomena within this kind of materials still remain difficult to predict: effective transport properties strongly depend on the volume fraction and the shape [1] of particles as well as on the particle-particle contact zones that may exhibit possible interfacial barriers and alter conduction [2–5]. They are also largely affected by the spatial distribution and the orientation of particles, both of them often being induced during the processing phase [6–9]. Likewise, because of the very high contrast between the conductivities of the matrix and the particles, predictions given by well-known bounds are usually less satisfactory for this kind of materials [10–12]. To circumvent the problem, a common assumption consists in neglecting the conduction phenomena in the matrix, except in the vicinity of particle-particle contacts. Within this framework, many models [13–31] have been obtained, some of them being especially dedicated to fibrous media [17,24–31]. They analyze the role of the volume fraction, the aspect ratio and the waviness of fibers on the effective transport properties. However, few of them have studied transient loadings as well as the roles of fiber-fiber contacts [27] and fiber orientation [30–32].

The goal of this study is to further analyze these aspects and to propose effective models for the transient diffusion in such fibrous media taking into account the quality of fiber-fiber contacts. In that respect, we have presented in paper I [39] a possible way to obtain the structure and the properties of the corresponding effective continua. For that purpose, the homogenization with multiple scale asymptotic expansions was used. Provided a good separation of scales between local heterogeneities and the macroscopic lengths of samples (or excitation), three equivalent macroscopic media have been identified, depending on the quality of particle-particle contacts. These continua obey the standard dimensionless macroscopic heat balance equation

$$c^{e*}\dot{T}^{e*} = -\nabla_{x^*}\cdot \mathbf{q}^{e*} + r^{e*}, \tag{1}$$

where the dimensionless macroscopic temperature T^{e*} is the first-order temperature of the asymptotic expansion of the temperature field, i.e., $T^{e*}=T^{[0]*}$, $\dot{T}^{e*}$ its rate, and where c^{e*} and r^{e*}, respectively, represent the effective volumetric heat capacity and external heat source. c^{e*} and r^{e*} are obtained by simply averaging local heat capacities (respectively, heat

*laurent.orgeas@hmg.inpg.fr

sources) over the whole volume of the considered representative elementary volume (REV). The macroscopic heat flow $\mathbf{q}^{e*}$ involved in the last equation follows a standard Fourier's law:

$$\mathbf{q}^{e*} = -\mathbf{\Lambda}^{e*} \cdot \boldsymbol{\nabla}_{x^*} T^{[0]*}, \tag{2}$$

where $\mathbf{\Lambda}^{e*}$ is the effective conductivity tensor. $\mathbf{\Lambda}^{e*}$ can be determined by solving steady state and linear localization problems on REV's. Such boundary value problems depend on the quality of fiber-fiber contacts.

For model III, contacts are highly resistive and the localization problem can be set in a reduced discrete form, i.e., it is a system of independent linear equations in which temperatures $\overline{T}_{\alpha}^{[1]*}$'s are unknown. On each fiber p_α (of center of mass G_α^*) contained in the REV, one must solve the following equation:

$$\sum_{\mathcal{C}_\alpha} \Gamma_{i\alpha\beta}^* \tilde{h}_{i\alpha\beta}^* (\Delta_{\alpha\beta} \overline{T}^{[1]*} + \mathbf{G}_\alpha^* \mathbf{G}_\beta^* \cdot \boldsymbol{\nabla}_{x^*} T^{[0]*}) = 0, \tag{3}$$

where the macroscopic temperature gradient $\boldsymbol{\nabla}_{x^*} T^{[0]*}$ is given and constant, $\Delta_{\alpha\beta} \overline{T}^{[1]*} = \overline{T}_\beta^{[1]*} - \overline{T}_\alpha^{[1]*}$, $\mathcal{C}_\alpha$ is the set of connections of particle p_α and where

$$\tilde{h}_{i\alpha\beta}^* = \frac{1}{\Gamma_{i\alpha\beta}^*} \int_{\Gamma_{i\alpha\beta}^*} h_{i\alpha\beta}^* dS^* \tag{4}$$

is the average of the heat transfer coefficient $h_{i\alpha\beta}^*$ on the surface $\Gamma_{i\alpha\beta}^*$ of the connection $i\alpha\beta$, i.e., the ith contact between particles p_α and p_β. Solving Eq. (3) then allows to compute the macroscopic heat flow with the following discrete expression, to be written over the set $\mathcal{C}_{\mathrm{REV}}$ of fiber-fiber connections contained in the REV (of volume Ω_{REV}^*):

$$\mathbf{q}^{e*} = -\frac{1}{\Omega_{\mathrm{REV}}^*} \sum_{\mathcal{C}_{\mathrm{REV}}} [\Gamma_{i\alpha\beta}^* \tilde{h}_{i\alpha\beta}^* (\Delta_{\alpha\beta} \overline{T}^{[1]*} + \mathbf{G}_\alpha^* \mathbf{G}_\beta^* \cdot \boldsymbol{\nabla}_{x^*} T^{[0]*}) \mathbf{G}_\alpha^* \mathbf{G}_\beta^*]. \tag{5}$$

For model I, contacts are highly conductive and the localization problem to be solved for each fiber p_α (of volume noted Ω_α^* and contact surface with the insulating matrix noted Γ_α^*) reads as

$$\boldsymbol{\nabla}_{y^*} \cdot \mathbf{q}_\alpha^{[1]*} = 0, \quad \text{in } \Omega_\alpha^*, \tag{6a}$$

$$\mathbf{q}_\alpha^{[1]*} = -\mathbf{\Lambda}_\alpha^* \cdot (\boldsymbol{\nabla}_{y^*} T_\alpha^{[1]*} + \boldsymbol{\nabla}_{x^*} T^{[0]*}) \quad \text{in } \Omega_\alpha^*, \tag{6b}$$

$$\mathbf{q}_\alpha^{[1]*} \cdot \hat{\mathbf{n}}_\alpha = 0 \quad \text{on } \Gamma_\alpha^*, \tag{6c}$$

$$T_\alpha^{[1]*} = T_\beta^{[1]*}, \quad \text{on } \Gamma_{i\alpha\beta}^*, \tag{6d}$$

$$\mathbf{q}_\alpha^{[1]*} \cdot \hat{\mathbf{n}}_{i\alpha\beta} = \mathbf{q}_\beta^{[1]*} \cdot \hat{\mathbf{n}}_{i\alpha\beta} \quad \text{on } \Gamma_{i\alpha\beta}^*, \tag{6e}$$

where $\boldsymbol{\nabla}_{y^*}$ is the differential operator with respect to the microscopic space variable $\mathbf{y}^*$, Γ_α^* is the surface of fibers in contact with the matrix, $\hat{\mathbf{n}}$ are external unit normal vectors to the considered surfaces. $\boldsymbol{\nabla}_{x^*} T^{[0]*}$ is still a constant and given and $T_\alpha^{[1]*}$ are the unknown temperatures to be determined within fiber p_α (of local conductivity tensor $\mathbf{\Lambda}_\alpha^*$). Solving system of Eqs. (6a)–(6e) then allows to compute the macroscopic heat flow

$$\mathbf{q}^{e*} = \langle \mathbf{q}_\alpha^{[1]*} \rangle = \frac{1}{\Omega_{\mathrm{REV}}^*} \sum_{\mathcal{P}_{\mathrm{REV}}} \int_{\Omega_\alpha^*} \mathbf{q}_\alpha^{[1]*} dV^*, \tag{7}$$

where $\mathcal{P}_{\mathrm{REV}}$ is the set of fibers in the REV.

For model II, which corresponds to the intermediate physical situation, the localization problem is identical to system of Eqs. (6a)–(6e), except for Eq. (6d) that must be replaced by

$$\mathbf{q}_\alpha^{[1]*} \cdot \hat{\mathbf{n}}_{i\alpha\beta} = -h_{i\alpha\beta}^* \Delta_{\alpha\beta} T^{[1]*} \quad \text{on } \Gamma_{i\alpha\beta}^*, \tag{8}$$

the expression of the effective heat flow (7) remaining unchanged.

It is then easy to see from Eqs. (2) and (5) [or system of Eqs. (6a)–(6e)] that $\mathbf{\Lambda}^{e*}$ can be estimated by imposing successively three unit independent macroscopic temperature gradients $\boldsymbol{\nabla}_{x^*} T^{[0]*}$. For example, when $\boldsymbol{\nabla}_{x^*} T^{[0]*} = \hat{\mathbf{e}}_1$, one obtains $\Lambda_{1i}^{e*} = -q_i^{e*}$ $(i \in \{1,2,3\})$. Also notice that for model III, the localization problem (3) is compact and discrete so that the numerical estimation of $\mathbf{\Lambda}^{e*}$ can be carried out quite easily with complex fibrous microstructures exhibiting a large number of fibers. Unfortunately, this is not the case for models I and II, where the localization problem (6a)–(6e) to be solved can rapidly become complicated and cumbersome.

The first objective of this paper is to reduce and simplify this localization problem, by accounting for the slender shape of fibers (Sec. II A). Physical assumptions can then be stated (Sec. II B) in order to obtain discrete formulations of the problem (6a)–(6e) (Sec. II C), the macroscopic heat flow (7) (Sec. II D) and the corresponding effective conductivity tensor (Sec. II E).

From the three discrete formulations, the second objective of the present work is to give numerical, semianalytical, and analytical estimates of the effective conductivity tensors. In that respect, the case of straight and monodisperse cylindrical fibers with circular cross section is then further explored. Semianalytical and analytical expressions of the effective conductivity tensors are obtained for highly conductive (model I) and highly resistive (model III) fiber-fiber contacts (Sec. II F). Therefrom, REV's with straight fibers are generated and used to solve numerically localization problems with discrete element codes (Sec. III). The influences of the quality of fiber-fiber contacts, the volume fraction of fibers, the orientation of fibers as well as the relative position and orientation of contacting fibers on the effective conductivity tensor are hence emphasized. Last, semianalytical and analytical predictions are compared with numerical results and their corresponding simplifying assumptions are discussed.

II. DISCRETE HOMOGENIZED FORMULATIONS

A. Geometrical assumptions

As shown in Fig. 1, we consider REV's (volume Ω_{REV}) made of P_{REV} slender and entangled wavy fibers p_α (volume Ω_α^*) of length l_α^* and constant cross section S_α^* (characteristic value S_c). The node $M_{i\alpha}^*$ refers to the projection on the center line of p_α of the ith contact point. The node $M_{i\beta}^*$ is defined

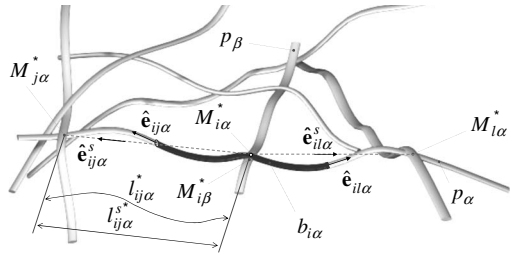

FIG. 1. Scheme of a REV (volume Ω^*_{REV}) made of P_{REV} slender and entangled wavy fibers p_α (volume Ω^*_α) of length l^*_α. Node $M^*_{i\alpha}$ refers to the projection on the center line of p_α of the ith contact point. $\hat{\mathbf{e}}_{ij\alpha}$ refers to the local unit vector tangent to the center line of fiber p_α between node $M^*_{i\alpha}$ and $M^*_{j\alpha}$, and $\hat{\mathbf{e}}^s_{ij\alpha}$ refers to the straight unit vector between these nodes. The darker part of fiber p_α represents the bar $b_{i\alpha}$.

similarly on the fiber p_β. At the ith contact point or connection noted $i\alpha\beta$ $(=i\beta\alpha)$, the distance between the center lines of two touching particles p_α and p_β is noted $d^*_{i\alpha\beta}=\|\mathbf{y}^*_{i\alpha\beta}\|=\|\mathbf{M}^*_{i\alpha}\mathbf{M}^*_{i\beta}\|$. The set of the C_{REV} connections $i\alpha\beta$ in the REV is noted $\mathcal{C}_{\mathrm{REV}}$ and that of the $\mathcal{C}_\alpha$ connections of fiber p_α is noted $\mathcal{C}_\alpha$. The external surface of a fiber p_α can be split in: Γ^*_α, the surface of the fiber in contact with the matrix, and $\Gamma^*_{i\alpha\beta}$, the surface of the ith contact in the REV, between fibers p_α and p_β. As shown in Fig. 1, the local unit vector tangent to the center line of fiber p_α between node $M^*_{i\alpha}$ and $M^*_{j\alpha}$ is noted $\hat{\mathbf{e}}_{ij\alpha}$. By noting $l^*_{ij\alpha}$ the length of the piece of fiber between these nodes and $\mathbf{y}^*_{ij\alpha}=\mathbf{M}^*_{i\alpha}\mathbf{M}^*_{j\alpha}=l^{s*}_{ij\alpha}\hat{\mathbf{e}}^s_{ij\alpha}$, the local waviness of the fiber is defined as $\xi^*_{ij\alpha}=l^*_{ij\alpha}/l^{s*}_{ij\alpha}$.

B. Physical assumptions for models I and II

In order to simplify the localization problem (6a)–(6e) it is now supposed that:

(1) Vector $\hat{\mathbf{e}}_{ij\alpha}$ tangent to the centerlines of the fibers is associated with the principal conductivity of the fibers $\Lambda^*_{\alpha I}$, further noted Λ^*_α and which is supposed as a constant along the fibers.

(2) Between nodes $M^*_{i\alpha}$ and $M^*_{j\alpha}$ of fiber p_α, the local heat flow $\mathbf{q}^{[1]*}_\alpha$ (6b) has a constant intensity and is parallel to the centerline of fiber p_α. The intensity of $\mathbf{q}^{[1]*}_\alpha$ is supposed to be equivalent to the intensity that would be in the *straight resistor* $M^*_{i\alpha}M^*_{j\alpha}$ of the same cross section S^*_α, length $l^{s*}_{ij\alpha}$, and conductivity $\Lambda^*_\alpha/\xi^*_{ij\alpha}$. Therefore, the heat flow $\mathbf{q}^{[1]*}_\alpha$ in the fiber p_α between $M^*_{i\alpha}$ and $M^*_{j\alpha}$, noted $\mathbf{q}^{[1]*}_{ij\alpha}$, can be estimated by

$$\mathbf{q}^{[1]*}_{ij\alpha} \approx -\frac{\Lambda^*_\alpha}{\xi^*_{ij\alpha}}\left(\frac{\Delta_{ij}T^{[1]*}_\alpha}{l^{s*}_{ij\alpha}} + \hat{\mathbf{e}}^s_{ij\alpha}\cdot\boldsymbol{\nabla}_{x^*}T^{[0]*}\right)\hat{\mathbf{e}}_{ij\alpha}. \tag{9}$$

(3) For model I, based on Eq. (6d), the first-order temperatures $T^{[1]*}_\alpha$ at nodes $M^*_{i\alpha}$ and $M^*_{i\beta}$ are supposed to be equal,

$$T^{[1]*}_{i\alpha} \approx T^{[1]*}_{i\beta}. \tag{10}$$

(4) For model II, based on Eq. (8), the dimensionless local heat flow $\mathbf{q}^{[1]*}_\alpha$ entering the bar $b_{i\alpha}$ through the contact zone $\Gamma^*_{i\alpha\beta}$ is noted $\mathbf{q}^{[1]*}_{i\alpha\beta}$ and is supposed as follows:

$$\mathbf{q}^{[1]*}_{i\alpha\beta} \approx -h^*_{i\alpha\beta}\Delta_{\alpha\beta}T^{[1]*}_i\hat{\mathbf{e}}_{i\alpha\beta}, \tag{11}$$

where $\hat{\mathbf{e}}_{i\alpha\beta}=\mathbf{y}^*_{i\alpha\beta}/\|\mathbf{y}^*_{i\alpha\beta}\|$.

When making such assumptions, a simple slender body model is achieved: the larger the lengths $l^*_{ij\alpha}$ with respect to the characteristic lengths of surfaces S^*_α and $\Gamma^*_{i\alpha\beta}$, the better the approximations (9)–(11).

C. Discrete form of the fluctuation problem for models I and II

As illustrated in Fig. 1, let us introduce the bar $b_{i\alpha}$, as the union of the second half of the piece of fiber between $M^*_{j\alpha}$ and $M^*_{i\alpha}$ and the first half of the piece of fiber between $M^*_{i\alpha}$ and $M^*_{l\alpha}$. This bar contains node $M^*_{i\alpha}$ and its neighbors are $b_{j\alpha}$ and $b_{l\alpha}$ that contain, respectively, nodes $M^*_{j\alpha}$ and $M^*_{l\alpha}$. The set of the B_α bars of p_α is noted $\mathcal{B}_\alpha$. Moreover, the junction $ij\alpha$ between bars $b_{i\alpha}$ and $b_{j\alpha}$ of the same fiber p_α is also introduced (the set of the J_α junctions $ij\alpha$ in p_α will be noted $\mathcal{J}_\alpha$, the set of the J_{REV} junctions $ij\alpha$ in the REV will be noted $\mathcal{J}_{\mathrm{REV}}$). Therefrom, the boundary value problem (6a)–(6e) in the bar $b_{i\alpha}$ is now considered: (i) integrating Eq. (6a) on the volume $\Omega^*_{i\alpha}$ of the bar $b_{i\alpha}$, (ii) using the divergence theorem, and (iii) accounting for the boundary conditions (6b), (6c), and (8) yield

$$\forall b_{i\alpha},\quad \int_{\Gamma^*_{ij\alpha}}\mathbf{q}^{[1]*}_{ij\alpha}\cdot\hat{\mathbf{e}}^s_{ij\alpha}dS^* + \int_{\Gamma^*_{il\alpha}}\mathbf{q}^{[1]*}_{il\alpha}\cdot\hat{\mathbf{e}}^s_{il\alpha}dS^* + \int_{\Gamma^*_{i\alpha\beta}}\mathbf{q}^{[1]*}_{i\alpha\beta}\cdot\hat{\mathbf{e}}_{i\alpha\beta}dS^* = 0. \tag{12}$$

By accounting for constitutive Eqs. (9) and (11), the last relation becomes

$$\forall b_{i\alpha},\quad \frac{\Lambda^*_\alpha S^*_\alpha}{\xi^*_{ij\alpha}}\left(\frac{\Delta_{ij}T^{[1]*}_\alpha}{l^{s*}_{ij\alpha}} + \hat{\mathbf{e}}^s_{ij\alpha}\cdot\boldsymbol{\nabla}_{x^*}T^{[0]*}\right) + \frac{\Lambda^*_\alpha S^*_\alpha}{\xi^*_{il\alpha}}\left(\frac{\Delta_{il}T^{[1]*}_\alpha}{l^{s*}_{il\alpha}} + \hat{\mathbf{e}}^s_{il\alpha}\cdot\boldsymbol{\nabla}_{x^*}T^{[0]*}\right) + \Gamma^*_{i\alpha\beta}\tilde{h}^*_{i\alpha\beta}\Delta_{\alpha\beta}T^{[1]*}_i = 0. \tag{13}$$

The last term on the left-hand side of Eq. (13) is vanishing in the case of model I, in accordance with Eq. (10). Expression (13) represents a system of $2C_{\mathrm{REV}}$ (C_{REV} for model I) linear equations to be solved for the calculation of the $2C_{\mathrm{REV}}$ (C_{REV} for model I) unknown temperatures $T^{[1]*}_{i\alpha}$. Such a system must be solved for three unit macroscopic temperature gradients $\boldsymbol{\nabla}_{x^*}T^{[0]*}=\hat{\mathbf{e}}_k$ $(k\in\{1,2,3\})$ and shows that the temperature fluctuation fields are linear functions of the macroscopic temperature gradient

$$\Delta_{ij}T^{[1]*}_\alpha = \Delta_{ij}\boldsymbol{\Theta}^{[1]*}_\alpha\cdot\boldsymbol{\nabla}_{x^*}T^{[0]*}$$

and

$$\Delta_{\alpha\beta}T^{[1]*}_i = \Delta_{\alpha\beta}\boldsymbol{\Theta}^{[1]*}_i\cdot\boldsymbol{\nabla}_{x^*}T^{[0]*}. \tag{14}$$

The components $(\boldsymbol{\Theta}^{[1]*}_{i\alpha})_k$ of the solution vector $\boldsymbol{\Theta}^{[1]*}_{i\alpha}$ correspond to the temperature fluctuations obtained at each node when $\nabla_{x^*}T^{[0]*}=\hat{\mathbf{e}}_k$.

Hence, by accounting for geometrical and physical assumptions and by using a finite volume technique, the continuous localization problem (6a)–(6e) is now written in a reduced discrete form.

D. Discrete form of the macroscopic heat flow for models I and II

By accounting for Eq. (6a) and by noting $\mathbf{y}^*_{i\alpha}=\mathbf{M}^*_{i\alpha}\mathbf{M}^*$, it is possible to write

$$\mathbf{q}^{[1]*}_{\alpha}=(\mathbf{y}^*_{i\alpha}\otimes\mathbf{q}^{[1]*}_{\alpha})\cdot\boldsymbol{\nabla}_{y^*}, \tag{15}$$

for all material points M^* in $b_{i\alpha}$. From this relation, by applying the divergence theorem and by using Eqs. (6b), (6c), and (8), the macroscopic heat flow $\mathbf{q}^{e*}$ defined in Eq. (7) can be set in the form

$$\mathbf{q}^{e*}=\frac{1}{\Omega^*_{\mathrm{REV}}}\sum_{\mathcal{P}_{\mathrm{REV}}}\sum_{\mathcal{B}_\alpha}\left(\int_{\Gamma^*_{ij\alpha}}(\mathbf{y}^*_{i\alpha}\otimes\mathbf{q}^{[1]*}_{ij\alpha})\cdot\hat{\mathbf{e}}_{ij\alpha}dS^*+\int_{\Gamma^*_{il\alpha}}(\mathbf{y}^*_{i\alpha}\otimes\mathbf{q}^{[1]*}_{il\alpha})\cdot\hat{\mathbf{e}}_{il\alpha}dS^*+\int_{\Gamma^*_{i\alpha\beta}}(\mathbf{y}^*_{i\alpha}\otimes\mathbf{q}^{[1]*}_{i\alpha\beta})\cdot\hat{\mathbf{e}}_{i\alpha\beta}dS^*\right). \tag{16}$$

By using the summation on the $ij\alpha$ junctions and on the $i\alpha\beta$ connections and by noticing $\mathbf{y}^*_{i\alpha}-\mathbf{y}^*_{i\beta}=\mathbf{y}^*_{i\alpha\beta}$ and $\mathbf{y}^*_{i\alpha}-\mathbf{y}^*_{j\alpha}=\mathbf{y}^*_{ij\alpha}$, the last expression now reads

$$\mathbf{q}^{e*}=\frac{1}{\Omega^*_{\mathrm{REV}}}\sum_{\mathcal{J}_{\mathrm{REV}}}\int_{\Gamma^*_{ij\alpha}}(\mathbf{y}^*_{ij\alpha}\otimes\mathbf{q}^{[1]*}_{ij\alpha})\cdot\hat{\mathbf{e}}_{ij\alpha}dS^*+\frac{1}{\Omega^*_{\mathrm{REV}}}\sum_{\mathcal{C}_{\mathrm{REV}}}\int_{\Gamma^*_{i\alpha\beta}}(\mathbf{y}^*_{i\alpha\beta}\otimes\mathbf{q}^{[1]*}_{i\alpha\beta})\cdot\hat{\mathbf{e}}_{i\alpha\beta}dS^*. \tag{17}$$

By accounting for Eqs. (14), (9), and (11), the discrete form of the macroscopic heat flow (17) can therefore be expressed as a standard Fourier's law,

$$\mathbf{q}^{e*}=-\boldsymbol{\Lambda}^{e*}\cdot\boldsymbol{\nabla}_{x^*}T^{e*}, \tag{18}$$

which discrete expressions of $\boldsymbol{\Lambda}^{e*}$ are given in the next section.

E. Discrete form of the effective conductivity tensor for all models

1. General expressions

From the discrete forms of the macroscopic heat flow [Eq. (17) for models I and II and Eq. (5) for model III], it is then possible to deduce a discrete formulation of the effective conductivity tensor for each model in case of media made of entangled slender and wavy fibers:

(i) In the case of model II, by introducing Eqs. (9) and (11) into Eq. (17), the effective conductivity tensor reads as

$$\boldsymbol{\Lambda}^{e*}=\boldsymbol{\Lambda}^{e*}_{\mathrm{fib}}+\boldsymbol{\Lambda}^{e*}_{\mathrm{cont}}, \tag{19}$$

with

$$\boldsymbol{\Lambda}^{e*}_{\mathrm{fib}}=\frac{1}{\Omega^*_{\mathrm{REV}}}\sum_{\mathcal{J}_{\mathrm{REV}}}\frac{\Lambda^*_\alpha S^*_\alpha l^{s*}_{ij\alpha}}{\xi_{ij\alpha}}\hat{\mathbf{e}}^s_{ij\alpha}\otimes\left(\frac{\Delta_{ij}\boldsymbol{\Theta}^{[1]*}_\alpha}{l^{s*}_{ij\alpha}}+\hat{\mathbf{e}}^s_{ij\alpha}\right) \tag{20}$$

and

$$\boldsymbol{\Lambda}^{e*}_{\mathrm{cont}}=\frac{1}{\Omega^*_{\mathrm{REV}}}\sum_{\mathcal{C}_{\mathrm{REV}}}\Gamma^*_{i\alpha\beta}\tilde{h}^*_{i\alpha\beta}d^*_{i\alpha\beta}\hat{\mathbf{e}}_{i\alpha\beta}\otimes\Delta_{\alpha\beta}\boldsymbol{\Theta}^{[1]*}_i. \tag{21}$$

Conductivity tensors $\boldsymbol{\Lambda}^{e*}_{\mathrm{fib}}$ and $\boldsymbol{\Lambda}^{e*}_{\mathrm{cont}}$ stand, respectively, for the contribution of the core of the fibers and the contribution of fiber-fiber contacts to the overall conductivity tensor $\boldsymbol{\Lambda}^{e*}$.

(ii) In the case of model I, when the quality of contacts is perfect, $\boldsymbol{\Lambda}^{e*}_{\mathrm{cont}}$ vanishes and $\boldsymbol{\Lambda}^{e*}=\boldsymbol{\Lambda}^{e*}_{\mathrm{fib}}$ by accounting for Eq. (10).

(iii) In the case of model III, when the quality of contacts is very poor, a discrete form of the effective conductivity tensor has directly been deduced from Eq. (5) (which has already been derived in paper I),

$$\boldsymbol{\Lambda}^{e*}=C_1\left(\frac{1}{C_{\mathrm{REV}}}\sum_{\mathcal{C}_{\mathrm{REV}}}\Gamma^*_{i\alpha\beta}\tilde{h}^*_{i\alpha\beta}\mathbf{y}^*_{\alpha\beta}\otimes(\mathbf{y}^*_{\alpha\beta}+\Delta_{\alpha\beta}\overline{\boldsymbol{\theta}}^{[1]*})\right), \tag{22}$$

where $\mathbf{y}^*_{\alpha\beta}=\mathbf{G}^*_\alpha\mathbf{G}^*_\beta$, C_1 is the number of fiber-fiber connections per unit of volume, and where the components $(\overline{\boldsymbol{\theta}}^{[1]*}_\alpha)_k$ of the solution vector $\overline{\boldsymbol{\theta}}^{[1]*}_\alpha$ correspond to the temperature fluctuations $\overline{T}^{[1]*}_\alpha$ when $\boldsymbol{\nabla}_{x^*}T^{[0]*}=\hat{\mathbf{e}}_k$.

2. Semianalytical expressions for models I and III

Considering the discrete localization problems (13) [respectively, Eq. (3) for model III], it is possible to show that for some types of regular fibrous arrangements, the temperature field at every contact points (respectively, at every centers of mass for model III) is an affine function of the position of the considered point in the REV. Supposing these assumptions can be stated for every microstructure (this will be discussed in Sec. III), the following semianalytical estimations of the conductivity tensors can be established.

In the case of model I, the affine assumption yields to suppose that $\Delta_{ij}\boldsymbol{\Theta}^{[1]*}_\alpha\approx\mathbf{0}$. From this hypothesis, the conductivity tensor can be estimated by

$$\boldsymbol{\Lambda}^{e*}=\boldsymbol{\Lambda}^{e*}_{\mathrm{fib}}\approx\sum_{\mathcal{P}_{\mathrm{REV}}}(\Lambda^*_\alpha\sum_{\mathcal{D}_\alpha}f_{ij\alpha}\hat{\mathbf{e}}^s_{ij\alpha}\otimes\hat{\mathbf{e}}^s_{ij\alpha}), \tag{23}$$

where $f_{ij\alpha}=S^*_\alpha l^{s*}_{ij\alpha}/(\xi_{ij\alpha}\Omega^*_{\mathrm{REV}})$ stands for the volume fraction of the piece of fiber p_α between nodes $M^*_{i\alpha}$ and $M^*_{j\alpha}$.

In the case of model III, the affine assumption, which is analogous to the one stated by Batchelor [13] in the case of spherical particles, reads as $\Delta_{\alpha\beta}\overline{\boldsymbol{\theta}}^{[1]*}\approx\mathbf{0}$. The conductivity tensor (22) then becomes

$$\boldsymbol{\Lambda}^{e*}\approx C_1\left(\frac{1}{C_{\mathrm{REV}}}\sum_{\mathcal{C}_{\mathrm{REV}}}\Gamma^*_{i\alpha\beta}\tilde{h}^*_{i\alpha\beta}\mathbf{y}^*_{\alpha\beta}\otimes\mathbf{y}^*_{\alpha\beta}\right). \tag{24}$$

Moreover, for slender fibers, it is fair to consider that

$$\mathbf{y}^*_{\alpha\beta}=s^*_{i\alpha}\hat{\mathbf{e}}_\alpha+2d^*_{i\alpha\beta}\hat{\mathbf{e}}_{i\alpha\beta}-s^*_{i\beta}\hat{\mathbf{e}}_\beta\approx s^*_{i\alpha}\hat{\mathbf{e}}_\alpha-s^*_{i\beta}\hat{\mathbf{e}}_\beta \tag{25}$$

noting $\mathbf{G}^*_\alpha\mathbf{M}^*_{i\alpha}=s^*_{i\alpha}\hat{\mathbf{e}}_\alpha$ and $\mathbf{G}^*_\beta\mathbf{M}^*_{i\beta}=s^*_{i\beta}\hat{\mathbf{e}}_\beta$. Hence, for slender fibers, the previous conductivity tensor can be approximated by

$$\mathbf{\Lambda}^{e*} \approx C_1 \left(\frac{1}{C_{\mathrm{REV}} \mathcal{C}_{\mathrm{REV}}} \sum \Gamma^*_{i\alpha\beta} \tilde{h}^*_{i\alpha\beta} \times (s^*_{i\alpha}\hat{\mathbf{e}}_\alpha - s^*_{i\beta}\hat{\mathbf{e}}_\beta) \otimes (s^*_{i\alpha}\hat{\mathbf{e}}_\alpha - s^*_{i\beta}\hat{\mathbf{e}}_\beta) \right). \quad (26)$$

Therefore, estimations (23), (24), and (26) only require the knowledge of the geometry of the fibrous microstructures. In the next section, their validity will be discussed from numerical results in the case of networks of disordered straight fibers. Finally, note that in the case of model II, no semianalytical expression can be obtained.

F. Straight, monodisperse, and homogeneously distributed fibers with circular cross section

In order to further simplify the above semianalytical expressions, let us now consider that fibers p_α are straight, with a constant length l^*_{fib}, a circular cross section of constant radius a^*, a constant averaged heat transfer coefficient $\tilde{h}^*$, a constant in-axis conductivity Λ^*_{fib}, and with an orientation vector noted $\hat{\mathbf{e}}_\alpha$. Moreover, let us assume that the considered fibrous microstructures are such that contact surfaces $\Gamma^*_{i\alpha\beta}$ are nearly identical, i.e., $\forall\ i\alpha\beta$, $\Gamma^*_{i\alpha\beta} \approx \Gamma^* = k\pi a^{*2}$, where k is a positive constant. Likewise, fibers are supposed to be homogeneously distributed in the REV. Hence, using, for instance, the statistical geometrical tube model [33–36], it is then possible to estimate the average number of connections per fiber,

$$\bar{C}_\alpha \approx 4f \left(\frac{l^*_{\mathrm{fib}}}{\pi a^*} \phi_1 + \phi_2 + 1 \right), \quad (27)$$

and the number of fiber-fiber connections per unit of volume in the REV,

$$C_1 \approx \frac{f}{2\pi a^{*2} l^*_{\mathrm{fib}}} \bar{C}_\alpha, \quad (28)$$

where $f = P_{\mathrm{REV}} \pi a^{*2} l^*_{\mathrm{fib}} / \Omega^*_{\mathrm{REV}}$ is the volume fraction of fibers and where the descriptors ϕ_1 and ϕ_2 can be estimated from the fiber orientation distribution function (ODF) set in its continuous form [35] or its discrete form [36], as done in this work,

$$\phi_1 = \frac{1}{P^2_{\mathrm{REV}}} \sum_{\mathcal{P}_{\mathrm{REV}}} \sum_{\mathcal{P}_{\mathrm{REV}}} \| \hat{\mathbf{e}}_\alpha \times \hat{\mathbf{e}}_\beta \|, \quad (29a)$$

$$\phi_2 = \frac{1}{P^2_{\mathrm{REV}}} \sum_{\mathcal{P}_{\mathrm{REV}}} \sum_{\mathcal{P}_{\mathrm{REV}}} |\hat{\mathbf{e}}_\alpha \cdot \hat{\mathbf{e}}_\beta|. \quad (29b)$$

It can be shown [35] that ϕ_1, respectively, equals $\pi/4$, $2/\pi$, and 0 when the orientation of fibers is three-dimensional (3D) random, two-dimensional (2D) random, and unidirectional, whereas ϕ_2, respectively, equals 1/2, $2/\pi$, and 1 for the same types of oriented microstructures.

1. Expressions of the effective conductivity tensors

Under the above assumptions, simpler expressions of effective conductivity tensors can be obtained.

In the case of model II, the effective conductivity tensor still reads as $\mathbf{\Lambda}^{e*} = \mathbf{\Lambda}^{e*}_{\mathrm{fib}} + \mathbf{\Lambda}^{e*}_{\mathrm{cont}}$. The core contribution (20) can be rewritten as

$$\mathbf{\Lambda}^{e*}_{\mathrm{fib}} = \Lambda^*_{\mathrm{fib}} \frac{\pi a^{*2}}{\Omega^*_{\mathrm{REV}}} \sum_{\mathcal{P}_{\mathrm{REV}}} \sum_{\mathcal{J}_\alpha} (l^*_{ij\alpha} \hat{\mathbf{e}}_\alpha \otimes \hat{\mathbf{e}}_\alpha + \hat{\mathbf{e}}_\alpha \otimes \Delta_{ij} \mathbf{\Theta}^{[1]*}_\alpha). \quad (30)$$

By introducing (i) the two extreme nodes $M^*_{i^-\alpha}$ and $M^*_{j^+\alpha}$ of the particle p_α, (ii) the length between the extreme nodes $l^*_{i^-j^+\alpha} = \Sigma_{\mathcal{J}_\alpha} l^*_{ij\alpha}$, which is the length of "the active part" of fiber p_α, (iii) $\tilde{l}^*$ as its average value over the whole REV, (iv) $k_\alpha = l^*_{i^-j^+\alpha} / \tilde{l}^*$, and (v) $\Delta_{i^-j^+} T^{[1]*}_\alpha$ the difference of the temperature fluctuations between the extreme nodes, Eq. (30) yields

$$\mathbf{\Lambda}^{e*}_{\mathrm{fib}} = \Lambda^*_{\mathrm{fib}} \frac{\pi a^{*2} \tilde{l}^*}{\Omega^*_{\mathrm{REV}}} \sum_{\mathcal{P}_{\mathrm{REV}}} k_\alpha \hat{\mathbf{e}}_\alpha \otimes \left(\hat{\mathbf{e}}_\alpha + \frac{\Delta_{i^-j^+} \mathbf{\Theta}^{[1]*}_\alpha}{k_\alpha \tilde{l}^*} \right). \quad (31)$$

As contacts on each fiber are supposed to be homogeneously distributed, it is fair to consider that $k_\alpha \approx 1$. By expressing the averaged active length of fibers $\tilde{l}^*$ as a function of both the length of fibers l^*_{fib} and the averaged number of connections per fiber, $\bar{C}_\alpha$, i.e.,

$$\tilde{l}^* = l^*_{\mathrm{fib}} \left(1 - \frac{1}{\bar{C}_\alpha} \right), \quad (32)$$

it becomes

$$\mathbf{\Lambda}^{e*}_{\mathrm{fib}} \approx f \left(1 - \frac{1}{\bar{C}_\alpha} \right) \Lambda^*_{\mathrm{fib}} \left(\mathbf{A} + \frac{1}{P_{\mathrm{REV}}} \sum_{\mathcal{P}_{\mathrm{REV}}} \hat{\mathbf{e}}_\alpha \otimes \frac{\Delta_{i^-j^+} \mathbf{\Theta}^{[1]*}_\alpha}{l^*_{\mathrm{fib}} \left(1 - \frac{1}{\bar{C}_\alpha} \right)} \right), \quad (33)$$

where

$$\mathbf{A} = \frac{1}{P_{\mathrm{REV}}} \sum_{\mathcal{P}_{\mathrm{REV}}} \hat{\mathbf{e}}_\alpha \otimes \hat{\mathbf{e}}_\alpha \quad (34)$$

stands for the second-order fiber orientation tensor [37]. The fiber-fiber contact contribution (21) simplifies to

$$\mathbf{\Lambda}^{e*}_{\mathrm{cont}} \approx 2C_1 k \pi a^{*3} \tilde{h}^* \frac{1}{C_{\mathrm{REV}} \mathcal{C}_{\mathrm{REV}}} \sum \pm \hat{\mathbf{e}}_{i\alpha\beta} \otimes \Delta_{\alpha\beta} \mathbf{\Theta}^{[1]*}_i, \quad (35)$$

where

$$\hat{\mathbf{e}}_{i\alpha\beta} = \pm \frac{\hat{\mathbf{e}}_\alpha \times \hat{\mathbf{e}}_\beta}{\| \hat{\mathbf{e}}_\alpha \times \hat{\mathbf{e}}_\beta \|}, \quad (36)$$

and the sign $\pm$ is chosen such that $\hat{\mathbf{e}}_{i\alpha\beta} \cdot \mathbf{y}_{\alpha\beta} > 0$. Combined with Eqs. (27) and (28), the above expressions underline the influences of the local physical properties Λ^*_{fib} and $\tilde{h}^*$, the geometry of fiber a^* and l^*_{fib}, the volume fraction of fibers f, and the orientation of fibers $\hat{\mathbf{e}}_\alpha$, $\mathbf{A}$, ϕ_1, and ϕ_2, on the effective conductivities.

In the case of model I, the effective conductivity tensor simplifies to $\mathbf{\Lambda}^{e*} = \mathbf{\Lambda}^{e*}_{\mathrm{fib}}$, i.e., to Eq. (33).

In the case of model III, under identical assumptions, and for fibers with a high aspect ratio, expression (26) becomes

$$\mathbf{\Lambda}^{e*} \approx C_1 k \pi a^{*2} \tilde{h}^* (\mathbf{\Psi}_1 + \mathbf{\Psi}_2 + \mathbf{\Psi}_3), \tag{37}$$

where

$$\mathbf{\Psi}_1 = \frac{1}{C_{\mathrm{REV}} \mathcal{P}_{\mathrm{REV}}} \sum C_\alpha \mathrm{I}^*_{G_\alpha} \hat{\mathbf{e}}_\alpha \otimes \hat{\mathbf{e}}_\alpha, \tag{38}$$

$$\mathbf{\Psi}_2 = -\frac{1}{C_{\mathrm{REV}} \mathcal{C}_{\mathrm{REV}}} \sum s^*_{i\alpha} s^*_{i\beta} (\hat{\mathbf{e}}_\alpha \otimes \hat{\mathbf{e}}_\beta + \hat{\mathbf{e}}_\beta \otimes \hat{\mathbf{e}}_\alpha), \tag{39}$$

$$\mathbf{\Psi}_3 = -\frac{1}{C_{\mathrm{REV}} \mathcal{C}_{\mathrm{REV}}} \sum (s^*_{i\alpha} \hat{\mathbf{e}}_\alpha - s^*_{i\beta} \hat{\mathbf{e}}_\beta) \otimes \Delta_{\alpha\beta} \overline{\boldsymbol{\theta}}^{[1]*}, \tag{40}$$

and

$$\mathrm{I}^*_{G_\alpha} = \frac{1}{C_\alpha} \sum_{\mathcal{C}_\alpha} (s^*_{i\alpha})^2. \tag{41}$$

By considering that $C_\alpha \approx \bar{C}_\alpha$ and that $I^*_{G_\alpha}$ does not depend on the particle p_α, i.e., $\forall\ \alpha, I^*_{G_\alpha} \approx I^*_G$, an estimation of $I^*_{G_\alpha}$ is

$$I^*_{G_\alpha} \approx I^*_G \approx \frac{l^{*2}_{\mathrm{fib}}}{12} \left(1 - \frac{1}{\bar{C}_\alpha}\right). \tag{42}$$

This finally yields to the above estimation of $\mathbf{\Psi}_1$,

$$\mathbf{\Psi}_1 \approx \frac{l^{*2}_{\mathrm{fib}}}{6} \left(1 - \frac{1}{\bar{C}_\alpha}\right) \mathbf{A}. \tag{43}$$

2. Analytical expressions for models I and III

By using the approximations adopted in Sec. II E 2 for the temperature fields, i.e., $\Delta_{i^- j^+} \mathbf{\Theta}^{[1]*}_\alpha \approx \mathbf{0}$ and $\Delta_{\alpha\beta} \overline{\boldsymbol{\theta}}^{[1]*} \approx \mathbf{0}$, respectively, for models I and III, and by accounting for Eqs. (27) and (28), it is possible to obtain very compact analytical estimations of conductivity tensors for fibrous microstructures displaying 3D-random ($\phi_1 = \pi/4, \phi_2 = 1/2$), 2D-random ($\phi_1 = 2/\pi, \phi_2 = 2/\pi$), and unidirectional ($\phi_1 = 0, \phi_2 = 1$) fiber orientation, but also if another ODF is given.

In the case of model I, the conductivity tensor (33) can be estimated by

$$\mathbf{\Lambda}^{e*} = \mathbf{\Lambda}^{e*}_{\mathrm{fib}} \approx f \left(1 - \frac{1}{\bar{C}_\alpha}\right) \Lambda^*_{\mathrm{fib}} \mathbf{A}, \tag{44}$$

In the case of model III, tensor $\mathbf{\Psi}_3$ Eq. (40) equals 0. Moreover, it will be assumed that $\mathbf{\Psi}_2 \approx 0$ (cf. next section). Therefore, Eq. (37) can be set in the form

$$\mathbf{\Lambda}^{e*} \approx C_1 k \pi a^{*2} \tilde{h}^* \frac{l^{*2}_{\mathrm{fib}}}{6} \left(1 - \frac{1}{\bar{C}_\alpha}\right) \mathbf{A}. \tag{45}$$

III. NUMERICAL ILLUSTRATIONS AND DISCUSSION

In this section, the influence of the volume fraction and the orientation of fibers on the previous discrete expressions of the macroscopic conductivity tensors is illustrated quantitatively. First, direct numerical calculations are performed using discrete element models (Sec. III A). Second, the relevance of the assumptions stated to derive the semianalytical (23) and (26), and the analytical expressions (44) and (45) is discussed (Sec. III B).

A. Discrete element models

In order to compute the effective conductivity tensors, cubic REV's of volume $l^{*3}_{\mathrm{REV}} = 5^3$ made of P_{REV} straight fibers (constant length $l^*_{\mathrm{fib}} = 5$) with a circular cross section (constant radius $a^* = 0.05$) were stochastically generated according to a methodology similar to that used in Ref. [36].

(i) Centers of mass G^*_α of each fiber p_α were ascribed to random positions in the REV.

(ii) Gaussian distributions of the orientation vectors $\hat{\mathbf{e}}_\alpha$ were then imposed. Here, three types of oriented microstructures were generated, the principal vectors $\hat{\mathbf{e}}_{\mathrm{I}}$, $\hat{\mathbf{e}}_{\mathrm{II}}$, and $\hat{\mathbf{e}}_{\mathrm{III}}$ of their corresponding orientation tensors $\mathbf{A}$ being, respectively, equal to $\hat{\mathbf{e}}_1$, $\hat{\mathbf{e}}_2$, and $\hat{\mathbf{e}}_3$: (i) isotropic microstructures with 3D-random fiber orientations, i.e., with $A_{\mathrm{I}} \approx A_{\mathrm{II}} \approx A_{\mathrm{III}} \approx 1/3$ [see Fig. 2(a)], (iii) nearly planar fibrous microstructures, i.e., with $A_{\mathrm{I}}/A_{\mathrm{II}} \approx 1$ and $A_{\mathrm{I}}/A_{\mathrm{III}} \approx 50$ [Fig. 2(b)], and (ii) nearly unidirectional fibrous microstructures, i.e., with $A_{\mathrm{II}}/A_{\mathrm{III}} \approx 1$ and $A_{\mathrm{I}}/A_{\mathrm{II}} \approx A_{\mathrm{I}}/A_{\mathrm{III}} \approx 20$ [Fig. 2(c)].

(iii) A connection between fibers p_α and p_β was detected and added to the set $\mathcal{C}_{\mathrm{REV}}$ as soon as p_α and p_β intersect. Moreover, we have simply assumed that the surface of contact $\Gamma^*_{i\alpha\beta} = \pi a^{*2}$ so that $k = 1$.

(iv) In order to estimate effective conductivity tensors for models I and III, the conductivity of the fibers Λ^*_{fib} as well as the heat transfer coefficient $\tilde{h}^*$ were both set arbitrarily to 1.

Thereby, a discrete element code that was initially developed to model the rheology of highly concentrated and non-Newtonian fiber-bundle suspensions [36,38], was modified in order to solve the two different linear localization problems (13) (with the last term equal to 0) and (3), respectively, associated with models I and III. Three calculations with independent unit macroscopic temperature gradients were necessary for each REV to obtain the $\Delta_{ij} \mathbf{\Theta}^{[1]*}_\alpha$'s for model I as well as the $\Delta_{\alpha\beta} \overline{\boldsymbol{\theta}}^{[1]*}$'s for model III. Computed values of the temperature fluctuations were then, respectively, introduced in Eqs. (30) and (26) in order to obtain numerical values of macroscopic conductivity tensors for models I and III. For each given set of microstructural parameters, the calculation was performed with 20 REV's. Notice that the same microstructures have also been used to estimate the conductivity tensor predicted by the semianalytical expressions (23) and (24), respectively, for model I and III. Finally, analytical expressions (44) and (45) have been estimated using two different methods to obtain descriptors ϕ_1 and ϕ_2: by computing Eqs. (29a) and (29b) with the discrete ODF's of the REV's, or by approximating them by their values for perfectly 3D-random, 2D-random, and unidirectional fiber orientation. These two ways of computing the analytical models will be referred to in the following as the *determinist* and *statistical* models, respectively.

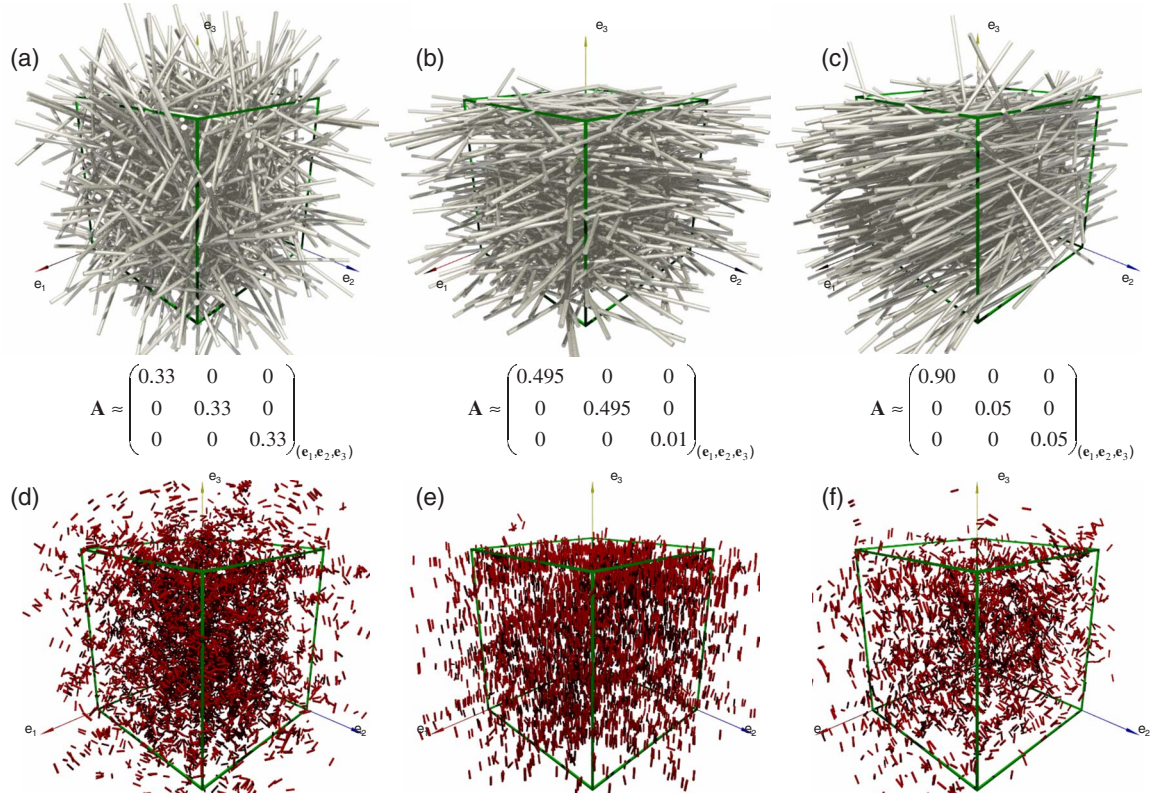

FIG. 2. (Color online) Examples of fibrous REV's generated numerically (fiber content $f=0.2$)—3D-random (a), nearly planar (b), and nearly unidirectional (c) fibrous networks with their corresponding orientation tensors $\mathbf{A}$. Cylinders plotted in the 3D views (d), (e), and (f) are, respectively, associated with fibrous networks (a), (b), and (c), they represent vectors normal to fiber-fiber contacts.

B. Results and discussion

Results given by numerical and (semi)analytical models are given in Figs. 3–5. In Fig. 3 the evolutions of the simulated principal effective conductivities $\Lambda_{\mathrm{I}}^{e*}$, $\Lambda_{\mathrm{II}}^{e*}$, and $\Lambda_{\mathrm{III}}^{e*}$ with f have been plotted for models I and III. In Figs. 4 and 5, the evolutions of the scalar quantities $\Lambda_{\mathrm{I}}^{e*}/A_{\mathrm{I}}$, $\Lambda_{\mathrm{II}}^{e*}/A_{\mathrm{II}}$ and $\Lambda_{\mathrm{III}}^{e*}/A_{\mathrm{III}}$, given by the numerical and (semi)analytical approaches, as functions of the volume fraction of fibers f have been sketched for models I (Fig. 4) and III (Fig. 5). Results have been obtained with isotropic [Figs. 3(a) and 3(b), Figs. 4(a) and 4(b), and Figs. 5(a) and 5(b)], nearly planar [Figs. 3(c) and 3(d), Figs. 4(c) and 4(d), and Figs. 5(c) and 5(d)] and nearly unidirectional [Figs. 3(e) and 3(f), Figs. 4(e) and 4(f), and Figs. 5(e) and 5(f)] fibrous networks. From these figures, the following comments can be established.

1. Influence of microstructure parameters

Numerical results plotted in the graphs of Fig. 3 first show that for REV's generated with the same microstructure parameters, the scattering of the results is rather weak (see the error bars). Consequently, only their mean values will be plotted in the other figures. Figure 3 also clearly emphasizes the leading role of both the fiber content and orientation on the Λ_i^{e*}'s. Whatever the fiber orientation, they also show that the increase of the Λ_i^{e*}'s with the fiber content is stiffer for model III than for model I. For example, in the very concentrated regime, i.e., approximately for $f \geq 0.1$, the Λ_i^{e*}'s tend to be linear and quadratic functions of the fiber content for model I and model III, respectively. Likewise, when $f \geq 0.1$, numerical results sketched in Figs. 4(a), 4(c), and 4(f) reveal that the anisotropy of the effective conductivity tensors for model I is closely linked with the anisotropy of the fiber orientation tensor: the Λ_i^{e*}/A_i (no summation on the index i) are nearly identical, whatever the considered index i. Notice that a similar trend was obtained for dilute fiber suspensions, i.e., for a local physics different from that studied here [30,32]. However, this trend is not systematically preserved, especially in the case of model III. For example, for almost unidirectional fibrous networks [Fig. 5(e)], when $f=0.4$, the values of $\Lambda_{\mathrm{I}}^{e*}/A_{\mathrm{I}}$ are approximately 50% lower than those recorded for $\Lambda_{\mathrm{III}}^{e*}/A_{\mathrm{III}}$ $(=\Lambda_{\mathrm{II}}^{e*}/A_{\mathrm{II}})$.

2. Numerical vs semianalytical solutions

Semianalytical estimations of the Λ_i^{e*}/A_i's have also been reported in Figs. 4(a), 4(c), and 4(e) and Figs. 5(a), 5(c), and 5(e). They follow the trends given by direct numerical results but overestimate them. In the concentrated regime, this deviation is fairly small (relative error $<25\%$) for isotropic as well as planar fibrous networks. By contrast, for almost unidirectional microstructures, the relative error becomes pronounced. For examples, when the fiber content varies from $f=0.1$ to $f=0.4$, the relative error decreases from $\approx 50\%$ to $\approx 10\%$ for model I and from $\approx 70\%$ to $\approx 15\%$ for model III. The observed discrepancies are ascribed to the forms stated

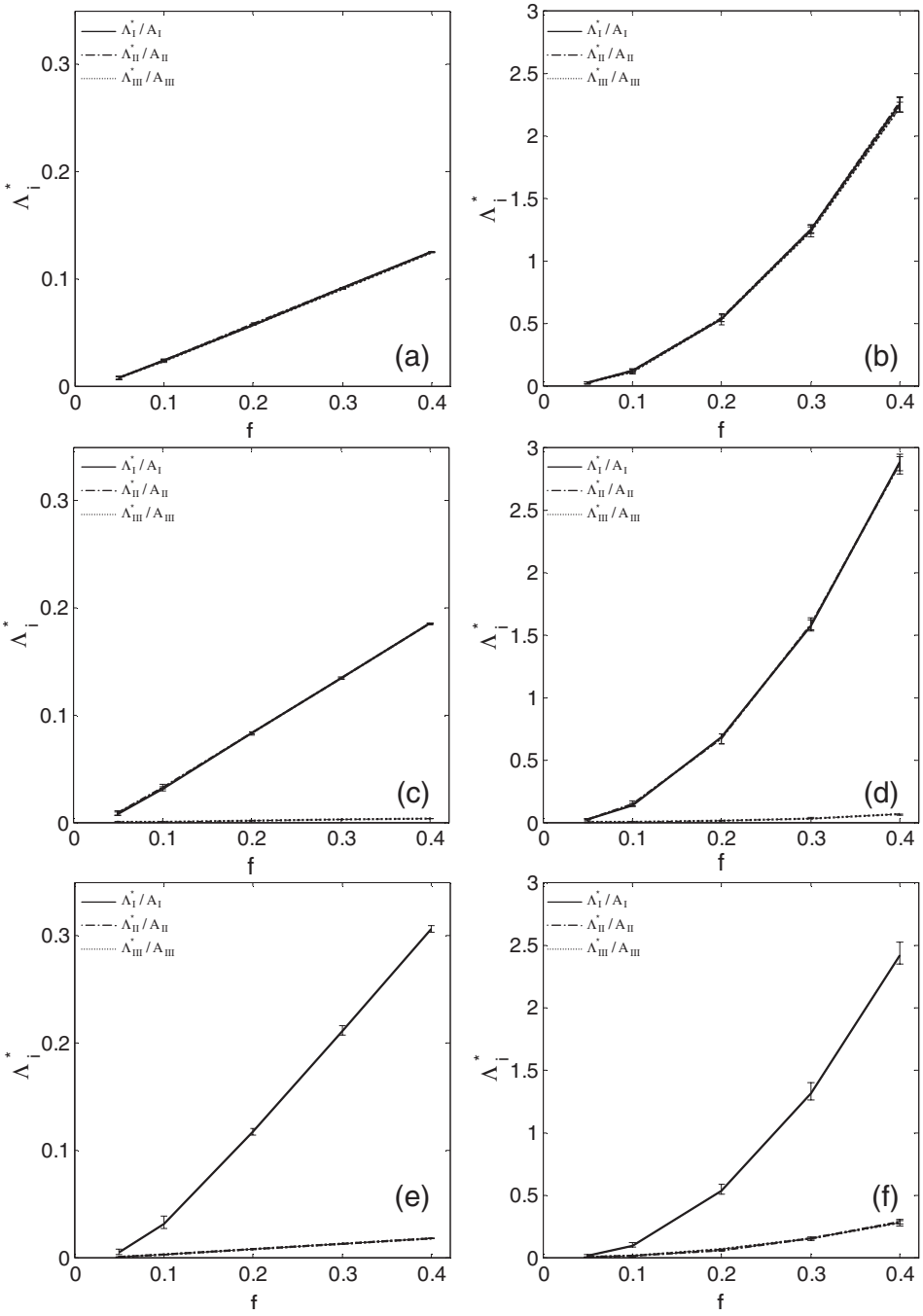

FIG. 3. *Direct numerical results*: Evolutions of the components Λ_I^{e*}, $\Lambda_{\mathrm{II}}^{e*}$, and $\Lambda_{\mathrm{III}}^{e*}$ of the effective conductivity tensor Λ^{e*} as functions of the fiber content f for 3D-random (a) and (b), nearly planar (c) and (d), and nearly unidirectional (e) and (f) microstructures. Numerical results with fibers' length $l_{\mathrm{fib}}^{*}=5$, fibers' radius $a^{*}=0.05$, and a unit thermal conductivity $\Lambda_{\mathrm{fib}}^{*}=1$ for model I (a)–(e) as well as a unit heat transfer coefficient $\tilde{h}^{*}=1$ for model III (b)–(f).

for temperature fields when establishing semianalytical models. To illustrate this, we have plotted in graphs of Fig. 6 the evolution of the local temperatures T_{α}^{*} at each center of bars for model I [Figs. 6(a) and 6(b)] and each center of fibers for model III [Figs. 6(c) and 6(d)], as functions of the centers' abscissa in the REV. In this figure, the fiber content is fixed to $f=0.3$ while isotropic and nearly unidirectional microstructures are considered. Temperatures obtained with direct numerical simulations (empty marks) are compared with an affine distribution of temperatures (lines), when REV's are subjected to a unit macroscopic temperature gradient along $\hat{\mathbf{e}}_1$. Lines corresponds to the assumption stated to derive semianalytical and analytical models, i.e., $\Delta_{ij}\boldsymbol{\Theta}_{\alpha}^{[1]*} \approx \mathbf{0}$ and $\Delta_{\alpha\beta}\overline{\boldsymbol{\theta}}^{[1]*} \approx \mathbf{0}$. As shown from this figure, the deviation of direct numerical results from the affine distribution is rather weak for isotropic fibrous networks: the mean deviation represents $\approx \pm 2\%$ of the mean temperature variation in the REV's for model I [Fig. 6(a)], and 2 times higher for model III [Fig. 6(c)]. By contrast, the affine distribution assumption becomes more questionable for nearly unidirectional fibrous networks, since the relative deviation is above $\pm 5\%$ for model I [Fig. 6(b)] and $\pm 10\%$ for model III [Fig. 6(d)]. Also notice that when the volume fraction of fibers increases, results show that deviations are decreasing faster for model I than for model III. This can explain why the relative error between numerical simulations and semianalytical calculations decreases slower for model III [Figs. 5(a), 5(c), and 5(e)] than for model I [Figs. 4(a), 4(c), and 4(e)].

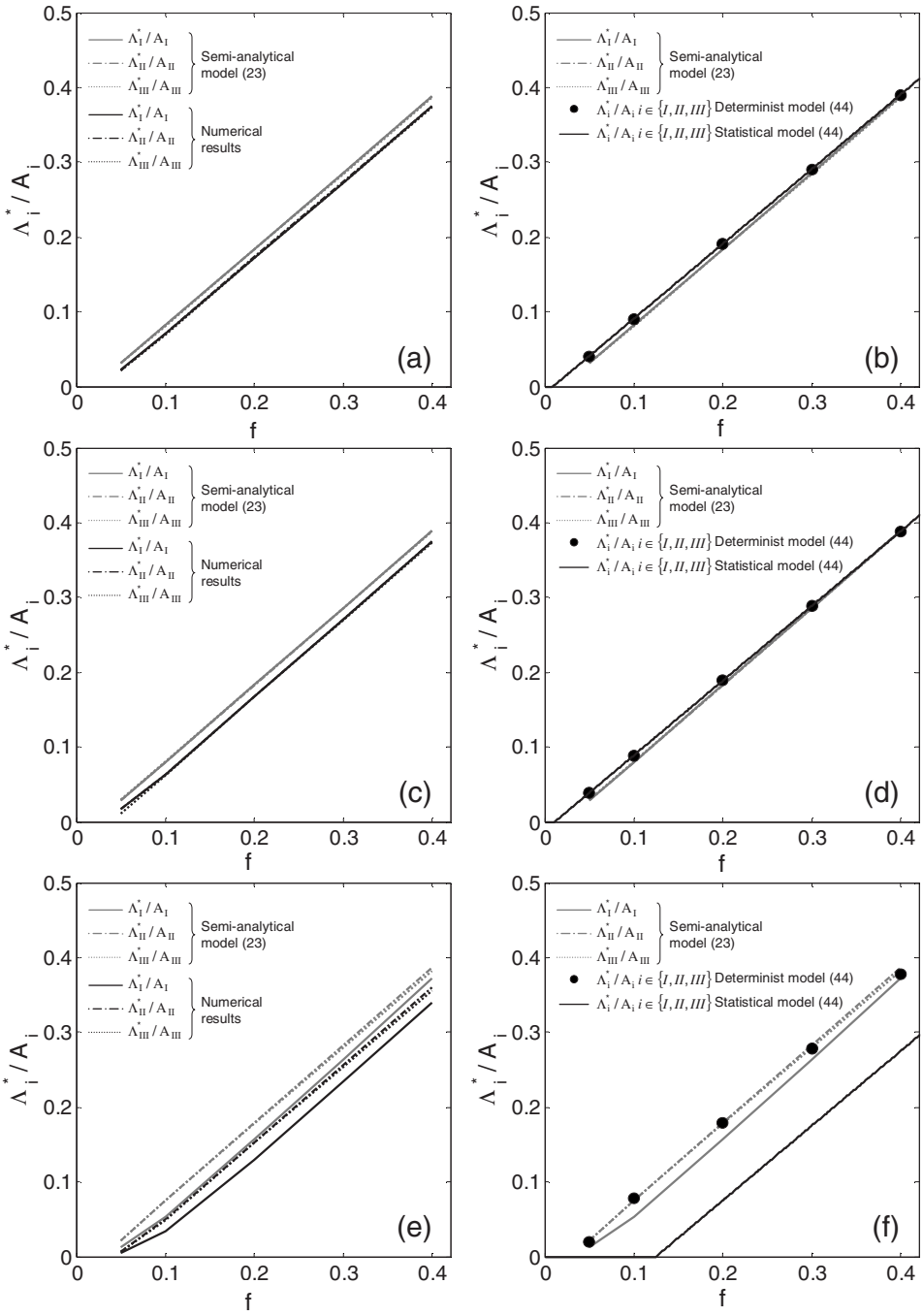

FIG. 4. *Model I*: Evolutions of the scalar Λ_i^{e*}/A_i's where $\mathbf{\Lambda}^{e*}$ is the effective conductivity tensor and $\mathbf{A}$ is the second-order orientation tensor. These evolutions are plotted as functions of the fiber content f for 3D-random (a) and (b), nearly planar (c) and (d), and nearly unidirectional (e) and (f). Comparison between semianalytical (gray lines) and numerical (black lines) (a)–(e) as well as between semianalytical (gray lines) and both determinist (black circles) and statistical (black lines) analytical estimations (b)–(f).

3. Semianalytical vs determinist expressions

Figures 4(b), 4(d), and 4(f) and Figs. 5(b), 5(d), and 5(f) show that semianalytical models (gray lines) are fairly well estimated by determinist models (black circles) at high fiber content ($f \geq 0.1$) with isotropic fibrous microstructures. This is still the case for model I with nearly planar and unidirectional microstructures [Figs. 4(d) and 4(f)]. For model III, determinist predictions (45) are less satisfactory for anisotropic microstructures, even if the general trend is preserved. In particular, the black circles cannot capture the difference of anisotropy recorded between the different directions (e.g. between continuous and dashed-dotted gray lines). We have checked that this discrepancy could not be ascribed to assumption (25) that has been used to establish analytical models. As an example, Fig. 7 represents semianalytical and analytical predictions for planar fibrous microstructures with different fiber aspect ratio $[5 \leq l_{\mathrm{fib}}^*/(2a^*) \leq 80]$ and a fiber content $f=0.2$. This figure shows that for slender fibers, i.e., when $l_{\mathrm{fib}}^*/(2a^*) \geq 40$, results obtained with the approximated semi-analytical model (26) (whites marks), i.e., with assumption (25), are almost superimposed with those obtained with the semianalytical model (24) (gray lines), i.e., without assumption (25), and do preserve the difference of anisotropy recorded between the different directions. Thus, assumption (25) is correct for slender fibers $[l_{\mathrm{fib}}^*/(2a^*) \geq 40]$ which are discussed in this section. By contrast, the same figure shows once again that the determinist analytical model (black

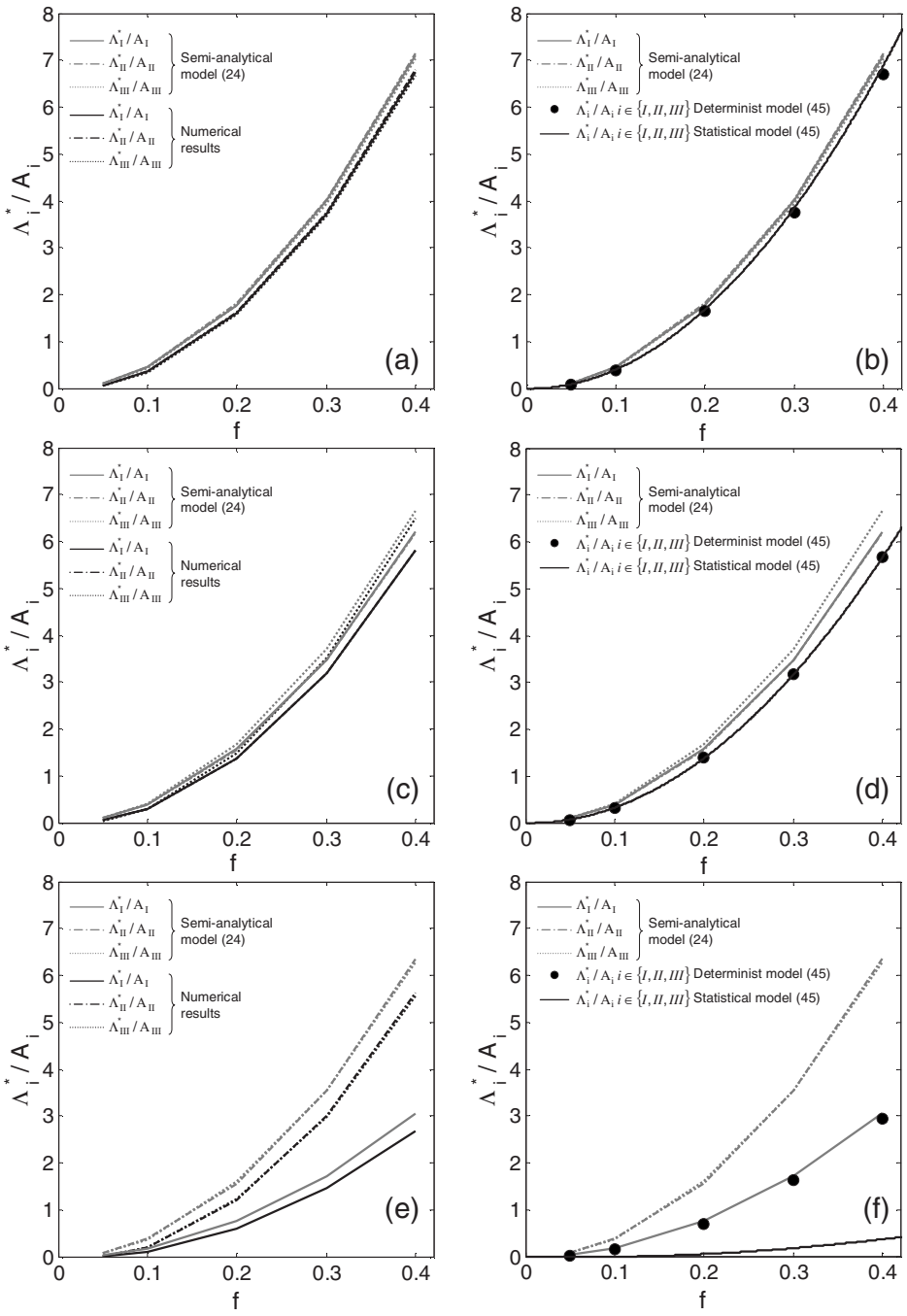

FIG. 5. *Model III*: Evolutions of the scalar Λ_i^{e*}/A_i's where $\mathbf{\Lambda}^{e*}$ is the effective conductivity tensor and $\mathbf{A}$ is the second-order orientation tensor. These evolutions are plotted as functions of the fiber content f for 3D-random (a) and (b), nearly planar (c) and (d), and nearly unidirectional (e) and (f). Comparison between semianalytical (gray lines) and numerical (black lines) (a)–(e) as well as between semianalytical (gray lines) and both deterministic (black circles) and statistical (black lines) analytical estimations (b)–(f).

circles) cannot capture these trends. Consequently, this tends to prove that tensor $\boldsymbol{\psi}_2$, which reflects the role of the relative position and orientation of connected fibers, and which has been neglected in order to obtain the analytical solution for model III, should not systematically be neglected in the expression of the effective conductivity tensor. It contributes to induce an additional anisotropy different from that induced by the fiber orientation tensor $\mathbf{A}$.

4. Determinist vs statistical solutions

The deterministic model (black circles) and the statistical model (black lines) follow the same evolution in the case of isotropic [Figs. 4(b) and 5(b)] and planar fibrous networks [Figs. 4(d) and 5(d)]. This shows that the as-generated REV's contain a sufficient number of fibers and follow the statistics of tube model. This is not the case for the nearly unidirectional fibrous microstructures [Figs. 4(f) and 5(f)]. The observed error is mainly ascribed to the fact that the descriptor ϕ_1 appearing in Eq. (27) was set to zero for the calculation of the statistical analytical estimation, whereas the generated fibrous networks are not perfectly unidirectional, i.e., their ϕ_1 is not exactly equal to 0. For the considered orientations and slender fibers, small variations of ϕ_1 near 0 can yield significant variations of $l_{\mathrm{fib}}^* \phi_1 / \pi a^*$, of $\bar{C}_\alpha$ and C_1, and consequently of the analytical predictions (44) and (45) used to determine the Λ_i^{e*}/A_i's.

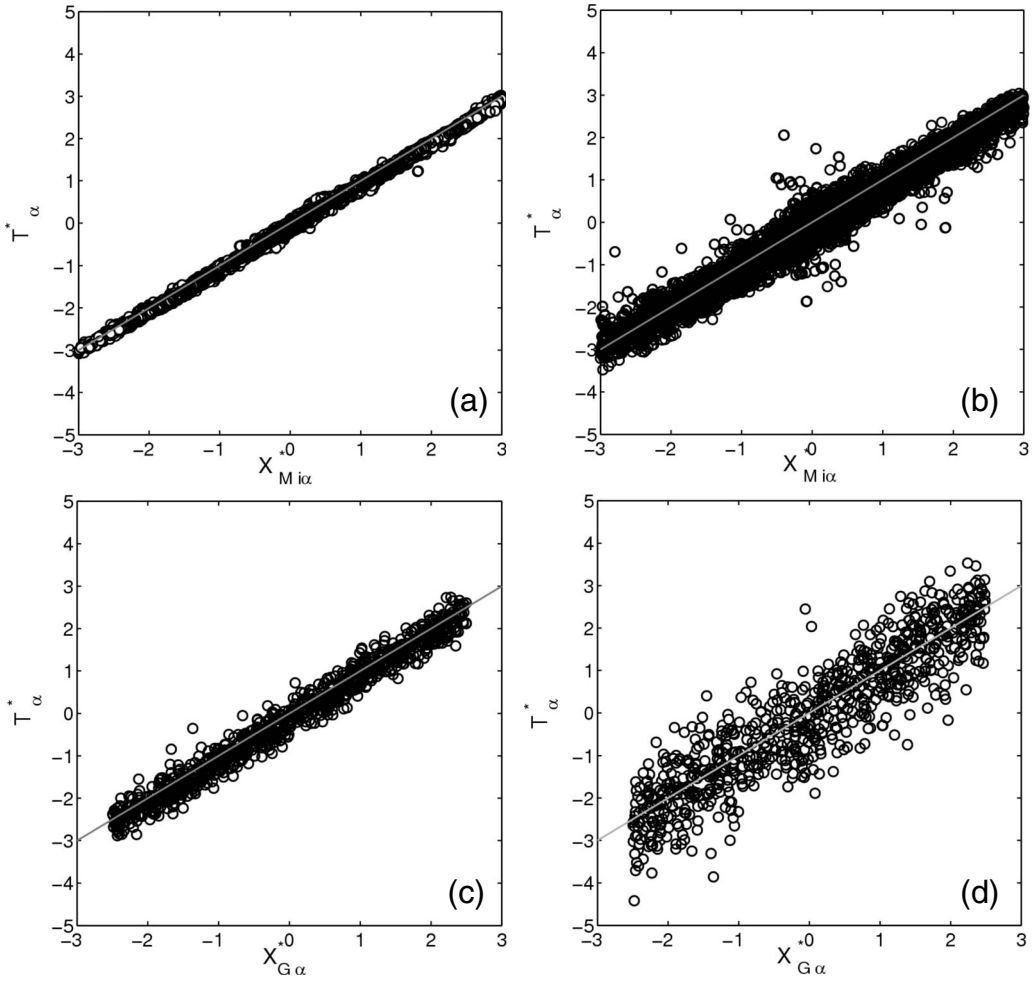

FIG. 6. Evolution of the temperature T^*_α with the abscissa of the centers of bars $X^*_{Mi\alpha}$ for model I (a) and (b) and with the abscissa of the centers of fibers $X^*_{G\alpha}$ for model III (c) and (d). Comparison between direct numerical results (empty marks) and affine distributions (lines) for isotropic (a) and (c) and unidirectional (b) and (d) microstructure.

IV. CONCLUDING REMARKS

When neglecting diffusion in the surrounding matrix, the transient diffusion through a network of connected conductive particles having interfacial barriers on their contacting zones have been studied theoretically with the homogenization method of multiple scale expansions in paper I of this contribution. Three different models have been obtained depending on the quality of fiber-fiber contacts: model I for highly conductive contacts, model III for highly resistive ones, and model II for intermediate situations. In this paper, we have proposed an application of these models for networks of slender and wavy fibers. Attention was focused on the calculation of the effective conductivity tensors, from localization problems established in paper I. The following points summarize the main results of this study.

(1) By accounting for the slender shape of fibers, simplifying physical assumptions have been stated for the conduction in and between fibers for models I and II. This allowed us to obtain discrete formulations of the localization problems and discrete expression of the effective conductivity tensors, as already presented for model III in paper I.

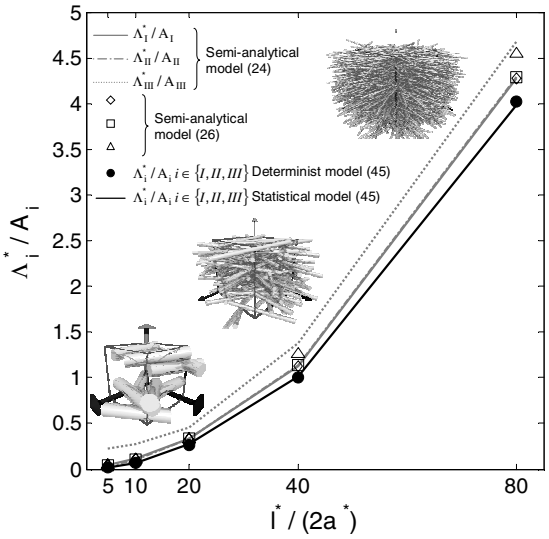

FIG. 7. Influence of the aspect ratio of fibers ($l^*_{\mathrm{fib}}/2a^*$) on semi-analytical (24) and (26) as well as analytical estimations (45) for planar microstructures with resistive contacts (model III) and fiber volume fraction $f=0.2$.

(2) Semianalytical expressions of the macroscopic conductivity tensors have been obtained for models I and III by fixing *a priori* the form of the temperature fields. These models only require the knowledge of the fibrous microstructures.

(3) Following the same procedure, analytical expressions of macroscopic conductivity tensors have also been proposed for models I and III in the case of straight, monodisperse, and homogeneously distributed cylindrical fibers with circular cross sections: (i) a determinist one for which it is only necessary to know the (discrete or continuous) orientation distribution function of fibers in order to estimate descriptors ϕ_1 and ϕ_2, (ii) a simplified one which gives direct results for isotropic, planar, and unidirectional fibrous microstructures.

(4) The effective conductivity tensors have also been computed using two discrete element codes, i.e., one for model I and another for model III. Results have emphasized the leading role of the fiber content on macroscopic conductivity tensors. Moreover, as the fiber content increases, these tensors tend to evolve like linear or quadratic functions of the fiber content when the quality of contact is excellent or poor, respectively. Likewise, numerical results have shown that the anisotropy of conductivity tensors was closely linked with the second-order fiber orientation tensor. Nonetheless, when fiber-fiber contacts are poor, numerical results have shown that the use of the second-order orientation tensor was not sufficient to capture the whole anisotropy of conductivity, especially in the case of nearly aligned microstructures.

(5) The proposed (semi)analytical estimations of the effective conductivity have been compared with numerical results. Semianalytical expressions give rather good approximations of the effective conductivity tensors for concentrated regimes. Their difference with numerical results remains within 70% whatever the orientation or the quality of contacts is, but within 40% if unidirectional microstructures at $f=0.1$ are not taken into account. Such error diminishes as the fiber and the quality of contact increase, and as the anisotropy of microstructures decreases. The determinist and the statistical analytical models give correct trends, despite their simplicity. Nevertheless, in the case of anisotropic microstructures and poor fiber-fiber contacts, they cannot capture the whole anisotropy of the conductivity tensor. In those cases, analytical models should account for the relative position and orientation of contacting fibers.

ACKNOWLEDGMENT

J.-P.V would like to thank the Region Rhone-Alpes (France) for its support to this work through a research grant.

[1] H. Tekce, D. Kumlutas, and I. Tavman, J. Reinf. Plast. Compos. **26**, 113 (2007).
[2] F. Dalmas, J.-Y. Cavaillé, C. Gauthier, L. Chazeau, and R. Dendievel, Compos. Sci. Technol. **67**, 829 (2007).
[3] H. Bhatt, K. Donaldson, and D. Hasselman, J. Am. Ceram. Soc. **73**, 312 (1990).
[4] A. Every, Y. Tzou, D. Hasselman, and J. Thomas, Acta Metall. Mater. **40**, 123 (1992).
[5] J. C. Geminard and H. Gayvallet, Phys. Rev. E **64**, 041301 (2001).
[6] Y. Agari, A. Ueda, and S. Nagai, J. Appl. Polym. Sci. **52**, 1223 (1994).
[7] R. Taipalus, T. Harmia, M. Zhang, and K. Friedrich, Compos. Sci. Technol. **61**, 801 (2001).
[8] F. Danes, B. Garnier, T. Dupuis, P. Lerendu, and T.-P. Nguyen, Compos. Sci. Technol. **65**, 945 (2005).
[9] P. Dumont, J.-P. Vassal, L. Orgéas, V. Michaud, D. Favier, and J.-E. Månson, Rheol. Acta **46**, 639 (2007).
[10] I. Webman, J. Jornter, and M. Cohen, Phys. Rev. B **11**, 2885 (1975).
[11] I. Kim and S. Torquato, J. Appl. Phys. **74**, 1844 (1993).
[12] J. Carson, S. Lovatt, D. Tanner, and A. C. Cleland, Int. J. Heat Mass Transfer **48**, 2150 (2005).
[13] G. Batchelor, F. O'Brien, and R. O'Brien, Proc. R. Soc. London, Ser. A **355**, 313 (1977).
[14] X. Zhuang, A. Didwana, and J. Goddard, J. Comput. Phys. **121**, 331 (1995).
[15] C. Argento and D. Bouvard, Int. J. Heat Mass Transfer **39**, 1343 (1996).
[16] G. Cheng, A. Yu, and P. Zulli, Chem. Eng. Sci. **54**, 4199 (1999).
[17] X. Cheng and A. M. Sastry, Mech. Mater. **31**, 765 (1999).
[18] W. Vargas and J. McCarthy, AIChE J. **47**, 1052 (2001).
[19] M. Bartkowiak and G. D. Mahan, Phys. Rev. B **51**, 10825 (1995).
[20] M. Sahimi, AIChE J. **39**, 369 (1993).
[21] M. Sahimi and T. Tsotsis, Ind. Eng. Chem. Res. **36**, 3043 (1997).
[22] S. Kirkpatrick, Rev. Mod. Phys. **45**, 574 (1973).
[23] M. Sahimi, *Heterogeneous Materials—Volumes I and II* (Springer-Verlag, New York, 2003).
[24] V. Favier, R. Dendievel, G. Canova, J.-Y. Cavaillé, and P. Gilormini, Acta Mater. **45**, 1557 (1997).
[25] L. Flandin, M. Verdier, B. Boutherin, Y. Brechet, and J.-Y. Cavaillé, J. Polym. Sci., Part B: Polym. Phys. **37**, 805 (1999).
[26] Z. Neda, R. Florian, and Y. Brechet, Phys. Rev. E **59**, 3717 (1999).
[27] F. Dalmas, R. Dendievel, L. Chazeau, J.-Y. Cavaillé, and C. Gauthier, Acta Mater. **54**, 2923 (2006).
[28] L. Berhan and A. M. Sastry, Phys. Rev. E **75**, 041120 (2007).
[29] L. Berhan and A. M. Sastry, Phys. Rev. E **75**, 041121 (2007).
[30] R. R. Sundararajakumar and D. L. Koch, J. Non-Newtonian Fluid Mech. **73**, 205 (1997).
[31] X. Cheng, A. M. Sastry, and B. E. Layton, J. Eng. Mater. Technol. **123**, 12 (2001).
[32] M. B. Mackaplow, E. S. G. Shaqfeh, and R. L. Schiek, Proc. R. Soc. London, Ser. A **447**, 77 (1994).
[33] M. Doi and S. F. Edwards, J. Chem. Soc., Faraday Trans. 2 **74**, 560 (1978).
[34] S. Ranganathan and S. G. Advani, J. Rheol. **35**, 1499 (1991).

[35] S. Toll, J. Rheol. **37**, 123 (1993).
[36] S. Le Corre, P. Dumont, L. Orgéas, and D. Favier, J. Rheol. **49**, 1029 (2005).
[37] S. G. Advani and C. L. Tucker, J. Rheol. **31**, 751 (1987).
[38] S. Le Corre, D. Caillerie, L. Orgéas, and D. Favier, J. Mech. Phys. Solids **52**, 395 (2004).
[39] J.-P. Vassal, L. Orgéas, D. Favier, J.-L. Auriault, and S. Le Corre, Phys. Rev. E **77**, 011302 (2008).